International Journal of Mechanical and Production Engineering Research and Development (IJMPERD)
ISSN (P): 2249-6890; ISSN (E): 2249-8001
Vol. 8, Issue 4, Aug 2018, 485-498

TRANS STELLAR
•Journal Publications •Research Consultancy

FLUID-STRUCTURE INTERACTION OF CROPPED DELTA WING WITH EXPERIMENTAL VALIDATION

ARUN. M. P[1], M. SATHEESH[2] & J. EDWIN RAJA DHAS[3]

[1]*Research Scholar, Department of Mechanical Engineering, Noorul Islam Centre for Higher Education, Tamil Nadu, India*

[2]*Assistant Professor, Department of Mechanical Engineering, Noorul Islam Centre for Higher Education, Tamil Nadu, India*

[3]*Professor, Department of Mechanical Engineering, Noorul Islam Centre for Higher Education, Tamil Nadu, India*

ABSTRACT

Fluid-structure interaction (FSI) is the commerce between a flexible structure and the surrounding fluid gives a variety of phenomenon. Application of this phenomenon in many areas like vibrational analysis of aircraft wings, machinery, bridges, etc. This computational analysis leads to many aerodynamic and structural dynamic problems. In the present article, we review the structural analysis of cropped delta wing aircraft with fence and without the fence. One of the key aspects of developing a better design from the data collected by FCI. Several such techniques are reviewed in this paper. As a part of this work, the experimental model setup for analysis the cropped delta wing by using wind tunnel and validate with software analysis values. The model of a cropped delta wing with the fence at different Mach number and angle of attack are selected to high spot the futuristic of computational problems.

KEYWORDS: Fluid-Structure Interaction, Wing fence, Angle of Attack & CFD

Received: Jun 29, 2018; **Accepted**: Jun 19, 2018; **Published**: Jul 16, 2018; **Paper Id.**: IJMPERDAUG201850

Original Article

1. INTRODUCTION

The wing of an aircraft has a major role in the aircraft, contributing all its lift produced to sustain in the air. The entire load of the aircraft including all the passenger, fuel, cargo, Artillery if it is a military aircraft, is been carried by the wings. So a tremendous amount of load is acting on the aircraft wing structure at all operational levels. To maintain its all-important aerodynamic shape, a wing must be designed and built to hold its shape even under extreme stress. Basically, the wing is a framework composed chiefly of spars, ribs, and (possibly) stringers [25].

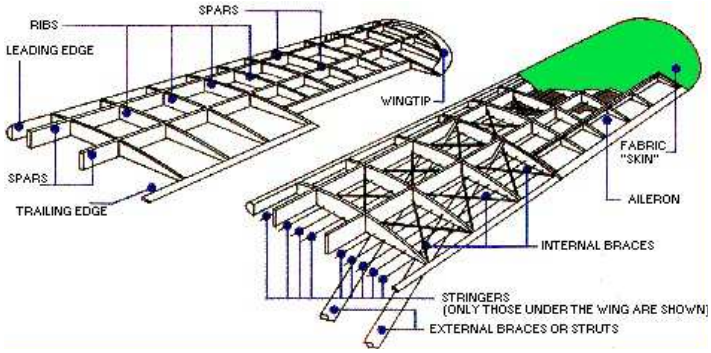

Figure 1: An Internal Structure of an Aircraft Wing

Spars are extended lengthwise of the wing (crosswise of the fuselage). In flight, the force of the air acts against the skin. From the skin, this force is transmitted to the ribs and then to the spars. The ribs are the parts of a wing which support the covering and provide the airfoil shape. Their purposes are providing shape, bearing flight stress, and these are called compression ribs [18].

It is a comparative study between the deformations due to the loads over the modified wing with the original. So the loads due to weight remain constant and only the aerodynamic loads have to be taken for the analysis. The Aerodynamics loads are obtained from the CFD analysis performed and results can be directly used in the structural analysis [4]. The most modern Computer Aided Engineering (CAE) technique called Fluid-Structure Interaction (FSI)[5] is applied. It is the interaction of some movable or deformable structure with an internal or surrounding fluid flow.

The second phase of this work is the testing of prototype model by using the wind tunnel. During a test, the model is placed in the test section of the tunnel and air is made to flow past the model. In some wind tunnel tests, flow visualization techniques are used to provide diagnostic information about the flow around the model [23]. Smoke is used to visualizing the flow that is away from the surface of the model. Smoke can be used to detect vortices and regions of separated flow. It can be injected from the surface or dispersed with a hollow wand that can be moved through the flow field. The disadvantage of smoke is that it does not work well at higher speeds (greater than ~300 mph), the smoke must be introduced at the proper location without altering the flow, and the smoke can leave a residue in the tunnel or on the model, depending on the type of smoke employed.

2. MATERIAL SELECTION

The main doubt about the metallic wing was regarding the kind of aluminum to be used in its components. In the metallic projects of conventional aviation there is a concern with the final price of the aircraft, therefore, in the areas of the components with less structural load, the aluminum used is of a less noble alloy and, thus cheaper. The mechanical properties of the aluminum depend on the width of the plate and orientation of the grains. For this work, in order to maintain the use of only one material, even when there is the reduction of the width of the skin or of the stringers throughout the span, it was decided to adopt a plate with an average width of 0.25” (6.35mm) to the whole model [4]. The orientation of the grains on the plate also influence the properties, the longitudinal orientation of the grains was chosen for it demonstrates a greater endurance than the others. The elastic isotropic properties and the mechanical properties of the Aluminum used are exposed in Table 1.

Table 1: Mechanical Properties of Aluminum

E (MPa)	G_{12} (MPa)	Ni_{12}	F_{tx} (MPa)	F_{ty} (MPa)	F_{cx} (MPa)	F_{cy} (MPa)
701016	26889	0.31	489	413	420	282

3. DESIGN AND FLUID STRUCTURE INTERACTION (FSI) ANALYSIS

The dimensions of the structure consist of a root chord of 8474.87 mm, a semi-span of 5500mm and a tip chord of 550.87 mm (Figure 2).

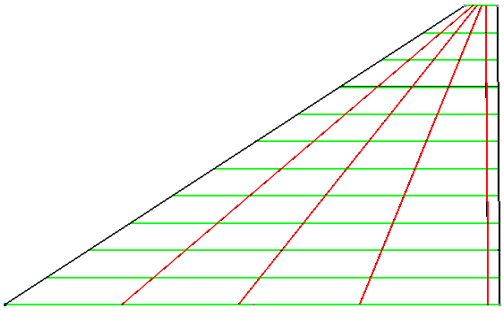

Figure 2: Spars and Ribs of a Wing

The Delta wing structure created using CATIA V5R21, was subjected to aerodynamic loads that are obtained from the CFD analysis [16]. The entire wing structure was constructed using 3mm sheet metal. The entire component created without any trimming in order to reduce the complexity of meshing and analysis. The four spars starting from the root rib and converging towards the tip rib.

The 12 ribs were placed uniformly over the span leaving a distance of 500mm between two ribs. The first spar was placed at 2000mm from the leading edge of the root rib. And next two spars placed at 2000mm from the nearest spar. The fourth and last spar placed at a distance of 2200mm from the third spar, equally carrying all the loads. A sheet metal skin of 3mm thickness was given to the entire structure.

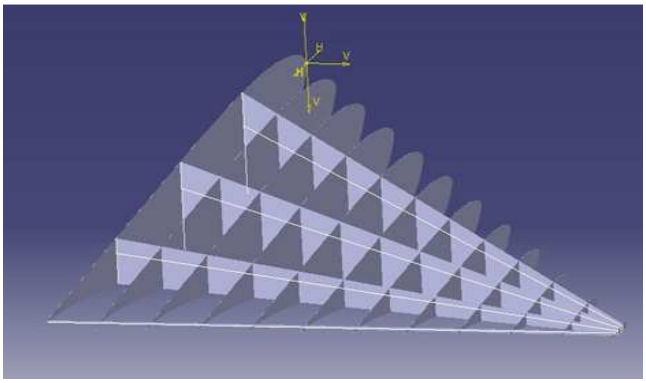

Figure 3: Wing Structure in Catia Software

3. 1. Meshing of the Wing Structure

The meshing was done in three steps. In the first step, the material Aluminum alloy was applied from the ANSYS Workbench Engineering Data section. Then the Structure was assembled into a single unit. In the final step, the Mechanical (Model) option in ANSYS Workbench was used to create a finite model. The maximum element size was

given as 100mm, the number of nodes are 287983 and number of elements are 140135.

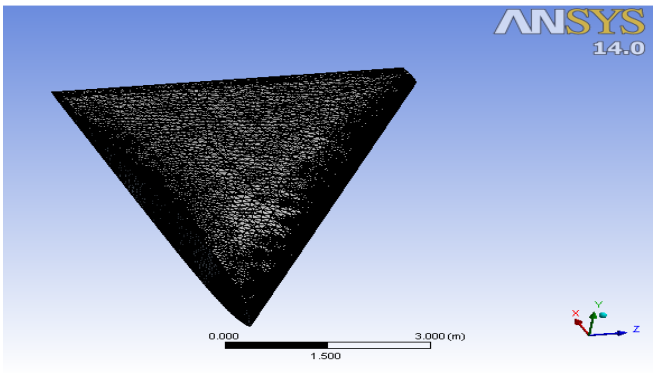

Figure 4: Wing Structure Meshing in ANSYS

Here the structure and CFD models are created separately and solved using Multi-physics. The results from CFD analysis are transferred into the structure analysis. The aerodynamic loads are imported as pressure and solved to get various results like total deformation, equivalent Stress, equivalent Elastic Strain and directional Deformation [24].

The FSI analysis was carried out at 0^0, 9^0,18^0 angles of attacks. The details of finite element model are given in Table 2.

Table 2: Finite Model Description

Object Name	Part 1	Part 2
State	Meshed	Meshed
Stiffness Behavior	Flexible	Flexible
Coordinate System	Default Coordinate System	Default Coordinate System
Reference Temperature	By Environment	By Environment
Material		
Assignment	Aluminum Alloy	Aluminum Alloy
Nonlinear Effects	Yes	Yes
Thermal Strain Effects	Yes	Yes
Bounding Box		
Length X	8.4765 m	
Length Y	0.85731 m	
Length Z	5.5 m	5.5033 m
Properties		
Volume	7.7715e-002 m^3	4.6761e-002 m^3
Mass	215.27 kg	129.53 kg
Centroid X	5.5737 m	4.618 m
Centroid Y	6.3928e-002 m	9.0979e-002 m
Centroid Z	1.8902 m	1.4773 m
Moment of Inertia Ip1	200.2 kg·m^2	124.34 kg·m^2
Moment of Inertia Ip2	894.56 kg·m^2	736.35 kg·m^2
Moment of Inertia Ip3	707.32 kg·m^2	620.04 kg·m^2
Statistics		
Nodes	206825	81158
Elements	103496	36639

3. 2. Structural Analysis of Wing without Fence

The figure 5 shows the loads imported from the CFD analysis. The minimum imported pressure was 0.3483 Pa that acts along the leading edge. The maximum pressure was 2225.5 Pa acting at the tip and at the wing fuselage

attachment part.

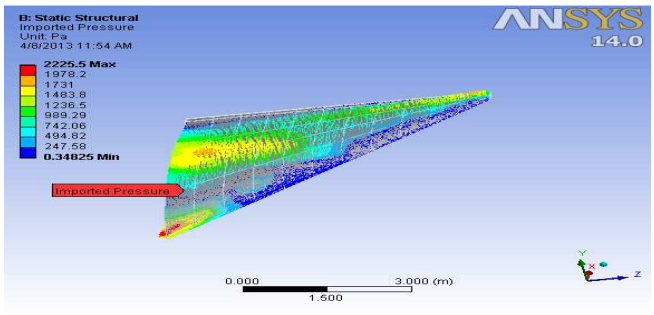

Figure 5: Pressure Distribution over the Wing Structure

The figure 6 shows the Total deformation of the wing structure under loading. The unit given is in the meter. The minimum deformation at the root given as $8.37x10^{-4}$ m. Along the lateral axis, the deformation increase and the maximum deformation occurs at the tip. The maximum deformation is noted to be $7.539x10^{-3}$ m.

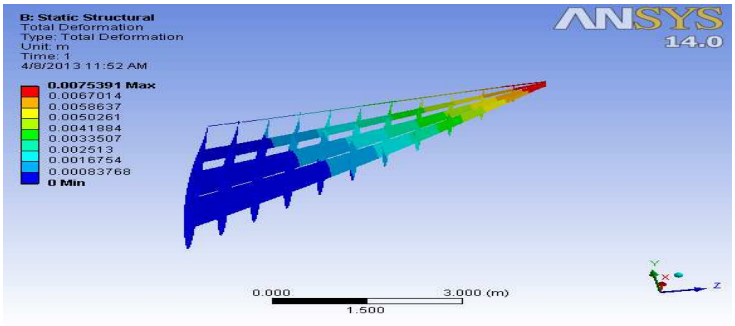

Figure 6: Total Deformation Over the Wing Structure

The figure 7 shows the Directional deformation of the wing structure under loading. The unit given is in the meter. The minimum deformation at the root given as $-8.564x10^{-5}$m. Along the lateral axis, the deformation increase and the maximum deformation occurs at the tip. The maximum deformation is noted to be $2.558x10^{-4}$ m.

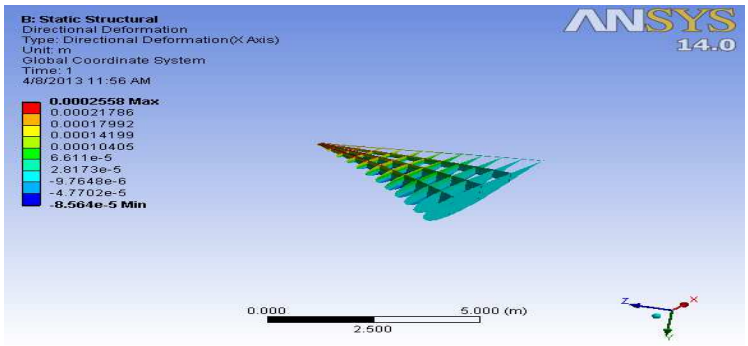

Figure 7: Directional Deformation over the Wing Structure

The figure 8 shows the Shear Elastic Strain of the wing structure under loading. The minimum deformation at the root given as $-2.7449x10^{-4}$. Along the lateral axis, the deformation increase and the maximum deformation occurs. The maximum deformation is noted to be $1.8921x10^{-3}$.

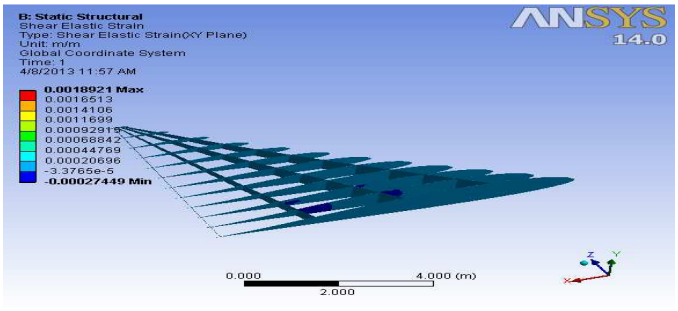

Figure 8: Shear Elastic Strain of the Wing

3. 3. Structural Analysis of Wing with Fence

The figure 9 shows the loads imported from the CFD analysis. The minimum imported pressure was 0.24186 Pa that acts along the leading edge. The maximum pressure was 2431.02 Pa acting at the tip and at the wing fuselage attachment part.

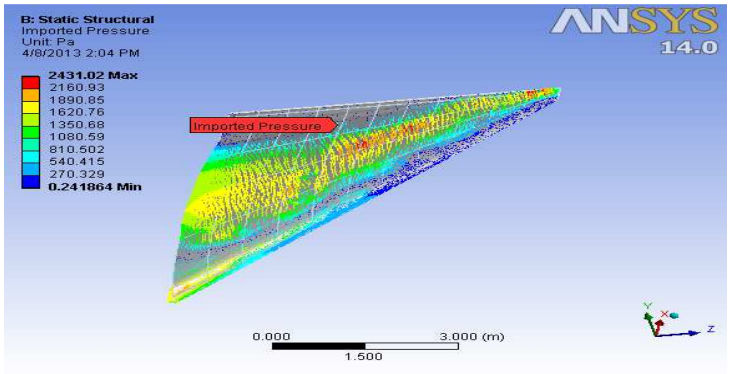

Figure 9: Pressure Distribution over the Wing Structure

The figure 10 shows the Total deformation of the wing structure under loading. The unit given is in the meter. The minimum deformation at the root given as $1.10x10^{-3}$ m. Along the lateral axis, the deformation increase and the maximum deformation occurs at the tip. The maximum deformation is noted to be $9.944x10^{-3}$ m.

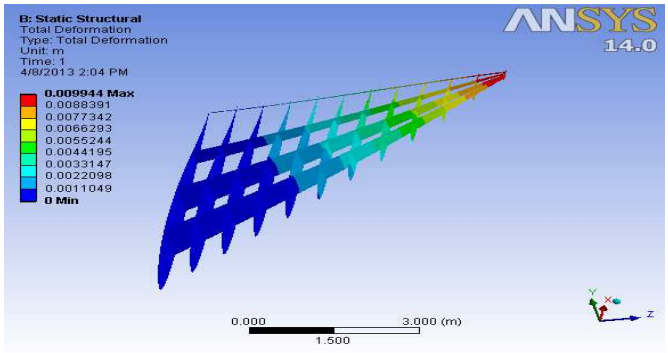

Figure 10: Total Deformation over the Wing Structure

The figure 11 shows the Directional deformation of the wing structure under loading. The unit given is in the meter. The minimum deformation at the root given as $-9.7551x10^{-5}$m. Along the lateral axis, the deformation increase and the maximum deformation occurs at the tip. The maximum deformation is noted to be $3.2203x10^{-4}$ m.

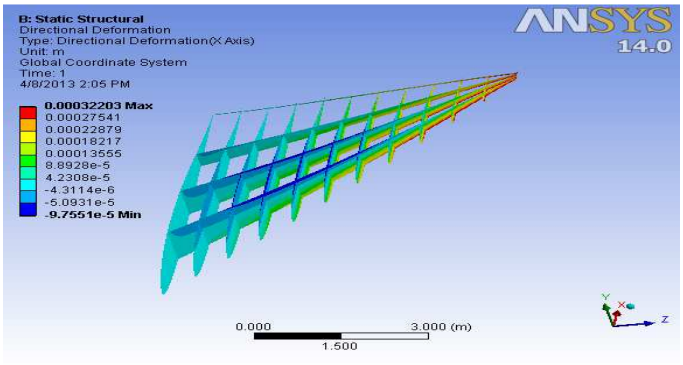

Figure 11: Directional Deformation over the Wing Structure

The figure 12 shows the Shear Elastic Strain of the wing structure under loading. The minimum deformation at the root given as -3.118×10^{-4}. Along the lateral axis, the deformation increase and the maximum deformation occurs. The maximum deformation is noted to be 2.231×10^{-3}.

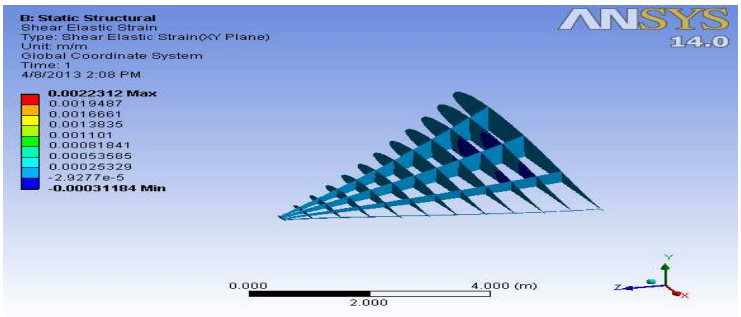

Figure 12: Shear Elastic Strain of the Wing

4. STATIC ANALYSIS OF FSI RESULT

The following tabulation depicts the comparative results of FSI analysis at three different angles say 0^o,9^o, and 18^o.

Table 3: Static Analysis of Wing without the Fence for an Angle of Attack 00

Results	Object Name			
	Total Deformation	Equivalent Stress	Equivalent Elastic Strain	Directional Deformation
Minimum	0. m	1.154e-010 Pa	0. m/m	-5.3546e-005 m
Maximum	4.3058e-003 m	5.7819e+007 Pa	8.1435e-004 m/m	1.5588e-004 m
Minimum Occurs On	Part 2			Part 1
Maximum Occurs On	Part 1	Part 2		Part 1

Table 4: Static Analysis of Wing with Fence for an Angle of Attack 00

Results	Object Name			
	Total Deformation	Equivalent Stress	Equivalent Elastic Strain	Directional Deformation
Minimum	0. m	4.444e-011 Pa	0. m/m	-6.8395e-005 m
Maximum	6.7434e-003 m	7.434e+007 Pa	1.047e-003 m/m	2.2553e-004 m
Minimum Occurs On	Part 2			Part 1
Maximum Occurs On	Part 1	Part 2		Part 1

Table 5: Static Analysis of Wing without Fence for an Angle of Attack 90

Results	Object Name				
	Total Deformation	Equivalent Stress	Equivalent Elastic Strain	Directional Deformation	Shear Elastic Strain
Minimum	0. m	5.3914e-011 Pa	0. m/m	-8.564e-005 m	-2.7449e-004 m/m
Maximum	7.5391e-003 m	8.8081e+007 Pa	1.2406e-003 m/m	2.558e-004 m	1.8921e-003 m/m
Minimum Occurs On	Part 2			Part 1	Part 2
Maximum Occurs On	Part 1	Part 2		Part 1	Part 2

Table 6: Static Analysis of Wing with Fence for an Angle of Attack 90

Results	Object Name			
	Total Deformation	Equivalent Stress	Equivalent Elastic Strain	Directional Deformation
Minimum	0. m	1.1721e-010 Pa	0. m/m	-9.7551e-005 m
Maximum	9.944e-003 m	1.0443e+008 Pa	1.4708e-003 m/m	3.2203e-004 m
Minimum Occurs On	Part 2			Part 1
Maximum Occurs On	Part 1	Part 2		Part 1

Table 7: Static Analysis of Wing without Fence for an Angle of Attack 180

Results	Object Name			
	Total Deformation	Equivalent Stress	Equivalent Elastic Strain	Directional Deformation
Minimum	0. m	7.4067e-011 Pa	0. m/m	-9.9138e-005 m
Maximum	8.8038e-003 m	9.8526e+007 Pa	1.3877e-003 m/m	2.9003e-004 m
Minimum Occurs On	Part 2			Part 1
Maximum Occurs On	Part 1	Part 2		Part 1

Table 8: Static Analysis of Wing with Fence for an Angle of Attack 180

Results	Object Name			
	Total Deformation	Equivalent Stress	Equivalent Elastic Strain	Directional Deformation
Minimum	0. m	6.7987e-011 Pa	0. m/m	-1.2279e-004 m
Maximum	1.2733e-002 m	1.2988e+008 Pa	1.8292e-003 m/m	4.0508e-004 m
Minimum Occurs On	Part 2			Part 1
Maximum Occurs On	Part 1	Part 2		Part 1

5. EXPERIMENTAL SETUP AND FLOW VISUALIZATION

For smoke visualization, the prototype was modeled with the following dimensions in CATIA V5R21. The CATIA drawing file was converted into step file, for the prototype to be machined. The method used was Synthetic Laser Sintering (SLS) process, a well-known rapid prototyping technique. An additive manufacturing layer technology SLS involves the use of a high power laser (for example, a carbon dioxide laser) to fuse small particles of plastic, metal (direct metal laser sintering), ceramic, or glass powders into a mass that has a desired three-dimensional shape. The laser selectively fuses powdered material by scanning cross-sections generated from a 3-D digital description of the part (for example from a CAD file or scan data) on the surface of a powder bed.

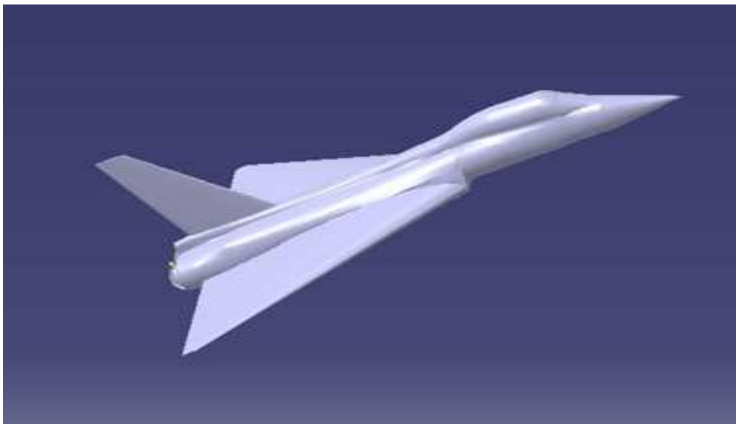

Figure 13: Designed Model of the Prototype in Catia V5R21

After each cross-section is scanned, the powder bed is lowered by one layer thickness, a new layer of material is applied on top, and the process is repeated until the part is completed. Because finished part density depends on peak laser power, rather than laser duration, an SLS machine typically uses a pulsed laser. The SLS machine preheats the bulk powder material in the powder bed somewhat below its melting point, to make it easier for the laser to raise the temperature of the selected regions the rest of the way to the melting point. The material used for prototype manufacturing is polyamide. Then the model is fixed into the wind tunnel with the following specification.

Table 9: Wind Tunnel Specifications

Parameter	Specifications
Test Section Size	600mm x 600mm x 4000mm.
Maximum Speed	45m/sec
Fan	Axial Flow fan of Diameter: 1.3 meter Maximum rpm: 1500 Number of Blades: 12 Hub Diameter: 500mm
Contraction Ratio	9: 1
Contraction length	1.8m
Settling chamber	1.8m×1.8m
Entry section	Bell mouthed entry
Honey Comb Size	50mm×50mm×450mm.
Screens	Two screens 8mesh and 16mesh stainless steel
Power	22 KW / 30HP AC motor, with speed control drive

5. 1. Smoke Visualization at Various Angles of Attacks

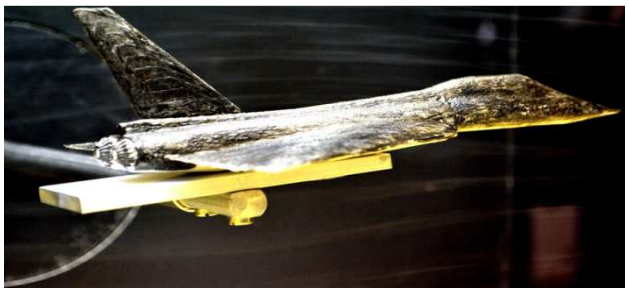

Figure 14: Smoke flow Visualization at an Angle of Attack90 (without Fences)

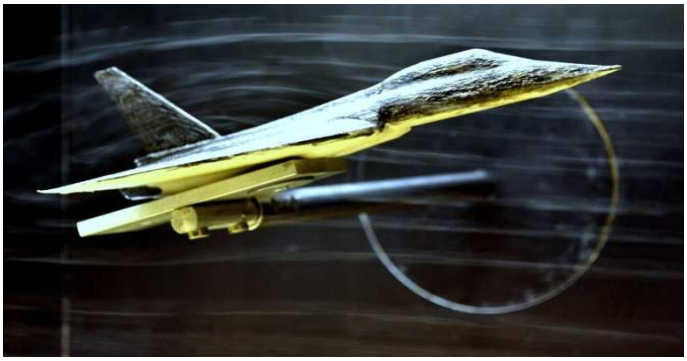

Figure 15: Smoke flow Visualization at the Angle of Attack 180(without Fences)

During the test, it has been found that the flow separation occurs at the angle of attack of 18^{o} as shown in figure 15.

It was observed that the flow separation for delta wing with fences only occurs after the angle of attack of 19.5^{o}. It was also found that the delta wing with fences possesses higher stall angle than the delta wing without fences.

Figure 16: Smoke flow Visualization at the Angle of Attack 90 (with Fences)

Figure 17: Smoke flow Visualization at an Angle of Attack 190 (with Fences)

5. 2. Aerodynamic Forces

Six Component strain gauge balance has been used to determine the forces such as lift, drag, pitching moment, rolling moment, side forces and yawing moments. The apparatus set up is done as per figure 18.

The setup is made and is placed in the wind tunnel and is tested at the velocity of 30m/sec at various angles of attack. The following table shows the lift and drags comparison at various angles of attack with and without wing fences.

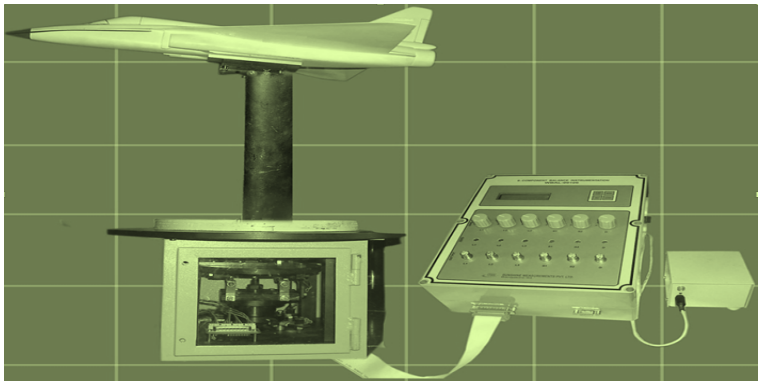

Figure 18: Experimental Setup for Force Determination

It can be noted from the graphs that even with a very slight increase in drag, the increase in lift of wing with fences is much higher than that without it and has higher stall angle.

Table 10: Comparison of Forces in with and without the Fence for Various Angles of Attack

Angle of Attack	Lift		Drag	
	Without Fence	With Fence	Without Fence	With Fence
0	0.589571	0.59945	0.091571	0.0962
3	0.601254	0.61923	0.104455	0.1069
6	0.61298	0.62475	0.1219	0.1325
9	0.6313	0.65841	0.1228	0.1395
18	0.72343	0.73232	0.128556	0.1435
19		0.7593		0.1484

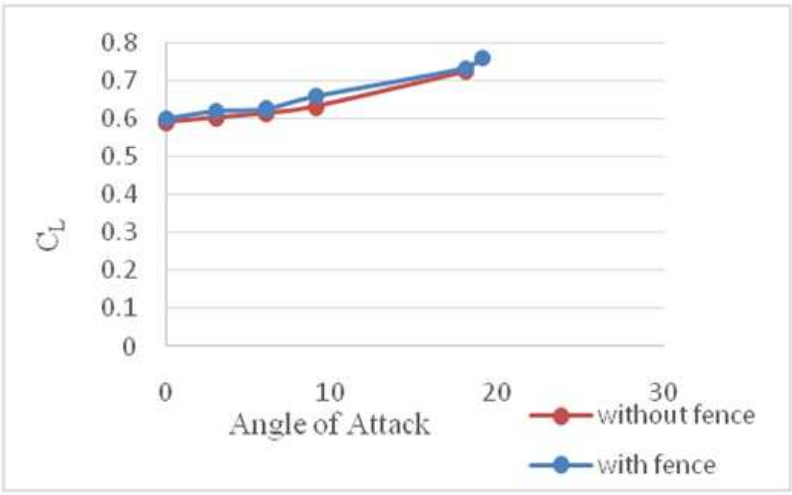

Figure 19: Variations of the Coefficient of Lift and Angle of Attack

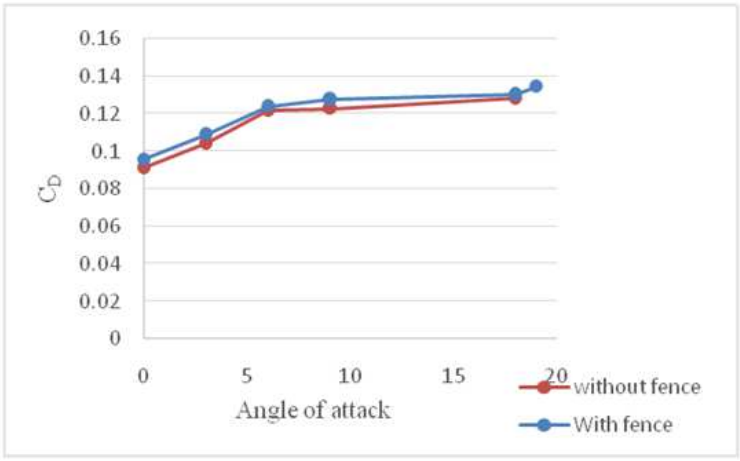

Figure 20: Variations of the Coefficient of Drag and Angle of Attack

6. CONCLUSIONS

This project has successfully validated the increased effectiveness of delta wing by the use of wing fences. Through the CFD environment, the C_L, C_D and the angle of attack values for delta wing with and without wing fences were generated and a comparative study was conducted. This unrevealed the increased lift characteristics of the delta wing with fences. The average increase in C_L is 13.03% with a small increment C_D in say 9%. The stall angle has increased by 1.535^o.

The modification in aerodynamic characteristics of the wing leads to increase in the lift which tends to increase the aerodynamic load over the wing thereby leading to structural deformation. In order to ensure the modification done produces negligible structural deformation, the aerodynamic load only is taken into consideration and the Fluid-Structural Interaction (FSI) analysis is done, from which a positive result has been obtained that the structure deforms by a very negligible value say 5-8% than that of the actual deformation.

In the real-time analysis a prototype was manufactured using Synthetic Laser Sintering (SLS) process using polyamide as material and was tested in a smoke tunnel, it was observed that the flow separation for delta wing with fences occurs only at a higher angle of attack than that without fences. It was also found that the delta wing with fences possesses higher stall angle than that without fences.

REFERENCES

1. *A Apashilkar – "Surface pressure model for simple delta wings at high angles of attack" Indian Academy of Science, Flight Mechanics & Control Division, National Aerospace Laboratories, Bangalore 560 017, India*
2. *Alexander Lippisch"The Delta wing: history and development", Iowa State University Press, 1981.*
3. *Anthony Mitchell and Scott Morton, Pascal Molton&Yair Guy – "Flow Control of Vertical Structures and Vortex Breakdown over Slender Delta Wings".*
4. *Arun. M. P and Dr. M. Satheesh "Analytical investigation of implementation of fences on cropped delta wing for the improvement of performance parameters" International Journal of Mechanical Engineering and Technology (IJMET) Volume 9, Issue 1, January 2018, pp. 538–548, ISSN Print: 0976-6340, Article ID: IJMET_09_01_058*
5. *BD Guo, QL Qu, JL Wu, PQ Liu "Fluid-structure interaction modeling by ALE and SPH" - Applied Mechanics and Materials, 2013*

6. *Bungartz, Hans-Joachim; Schäfer, Michael, eds. (2006).'Fluid-structure Interaction: Modelling, Simulation, Optimization'Springer-Verlag. ISBN3540-34595-7.*
7. *Chao, D. D., and van Dam, C. P., "Airfoil Prediction and Decomposition," AIAA Paper 98-2783.*
8. *Christopher Pevitt and Firoz Alam – "Static Computational Fluid Dynamics Simulations around a Specialised Delta Wing". DOI: 2014.04.025*
9. *Erik Conway (1945) 'High-Speed Dreams: NASA and the Technopolitics of Supersonic Transportation' JHU Press, ISBN:1421410435, 9781421410432*
10. *G. J. Van Wylen and R. E. Sonntag 'Fundamentals of Classical Thermodynamics', 1966, 43 (5), p A472*
11. *Giles, Michael B. and Cummings, Russell M., "Wake Integration for Three- Dimensional Computations: Theoretical Developments," Journal of Aircraft, Vol. 36, No. 2, 1996, pp. 357-365.*
12. *Groover (2001) 'CAD/CAM: Computer-Aided Design and Manufacturing' Pearson Education India SBN: 8177584162, 9788177584165*
13. *H. Wittenberg Springer (2009) 'Flight Physics: Essentials of Aeronautical Disciplines and Technology, with Historical Notes' ISBN: 1402086644, 9781402086649*
14. *Sakana, G., and B. Kaleeswari. "Enhancing Energy Efficiency of Sram through Optimization of SRAM Array Structures."*
15. *Hunt, David L., Cummings, Russell M. and Giles, Michael B., "Determination of Drag from Three-Dimensional Viscous and In viscid Flowfield Computations," AIAA Paper 97-2257, June 1997*
16. *Ira H. Abbott and Albert E. Von Doenhoff, "Theory of Wing Sections", Dover Publishing, New York, 1951.*
17. *Tailor, Mr. "Approaches To Modeling Unstable Flow And Mixing Of Variable Of Density Fluids."*
18. *J. Watson – "Calculation of Derivatives for a Cropped Delta Wing with Subsonic Leading Edges Oscillating in a Supersonic Air Stream", 1956.*
19. *Jin Y., Yuan X., Shin B. R., "Numerical Analysis of the Airfoil's Fluid-Structure Interaction Problems at Large at Large Mean Incidence Angle", Proc. ICCFD, Sydney, Australia, 15–19 July 2002.*
20. *John David Anderson (Jr) (1985) 'FUNDAMENTALS OF AERODYNAMICS' Tata McGraw-Hill Education, ISBN: 0070700125, 9780070700123*
21. *Karna S. Patel, Saumil B. Patel, Utsav B. Patel, Prof. Ankit P. Ahuja "CFD Analysis of an Aerofoil" International Journal of Engineering Research Volume No.3, Issue No.3, pp : 154 -158, ISSN:2319-6890)(online),2347-5013(print) 01 March 2014*
22. *M. Fairuz, M. Z Abdulla, H Yousuff and M. K Abdullah -"Fluid Structural Interaction of Unsteady Aerodynamics", 2013*
23. *Michael D. Williams, Mark F. Reeder, Raymond C. Maple, and Daniel A. Solfelt - "Modeling, Simulation, and Flight Tests for a T-38 Talon with Wing Fences". DOI: 10.2514/1.46122*
24. *Ronald, B. "Antibiogram of Klebsiella Sp. Isolated from Ascitic Fluid of Pyometra Infected Rottweiler Canine." (2016).*
25. *Michael V. Ol & Morteza Gharib – "Leading-Edge Vortex Structure of Nonslender Delta Wings at Low Reynolds Number".*
26. *Michel Joël Tchatchueng Kammegne, Lucian Teodor Grigorie, Ruxandra Mihaela Botez, Andreea Koreanschi, "Design and wind tunnel experimental validation of a controlled new rotary actuation system for a morphing wing application", Volume: 230 issue: 1, page(s): 132-145, Proceedings of the Institution of Mechanical Engineers, Part G: Journal of Aerospace Engineering, 2015.*

27. *Prabhakar A. and Ohri A., "CFD Analysis on MAV NACA 2412 Wing in High Lift Take-Off Configuration for Enhanced Lift Generation", J Aeronaut Aerospace Eng., 2:125. doi:10.4172/2168-9792.1000125, 2013.*
28. *Q Qu, W Wang, P Liu, RK Agarwal "Airfoil aerodynamics in ground effect for wide range of angles of attack"- AIAA Journal, 2015Z.*
29. *Thakur, M. O. H. I. T., D. Gangacharyulu, and G. U. R. P. R. E. E. T. Singh. "Effect of temperature and multiwalled carbon nanotubes concentration on thermophysical properties of water base nanofluid." IJE Trans. B Appl 30.8 (2017): 1223-30.*
30. *Q Qu, Z Lu, H Guo, P Liu, RK Agarwal "Numerical investigation of the aerodynamics of a delta wing in ground effect" - Journal of Aircraft, 2014*
31. *Lohakare, Sandhya. "Objectively structured clinical evaluation (OSCE) versus conventional examination method used for dental postgraduates students in practical." Internafional Journal of Management, Informafion Technology and Engineering 3.9 (2015): 23-30.*
32. *R. Gordon & J. Rom – "Calculation of Nonlinear Subsonic Characteristics of Wings with Thickness and Camber at High Incidence"*
33. *Robert C. Nelson, Alain Pelletier – "The unsteady aerodynamics of slender wings and aircraft undergoing large amplitude manoeuvres".*
34. *Stefan Wiggen, German Aereospace Center (DLR), Institute of Aeroelasticity, Bunsenstrasse 10, 37073 Göttingen, Germany- 'Unsteady pressure distributions at the wind tunnel model of a pitching Lambda wing with development of vortical flow'.12 October 2015-Elsevier*
35. *T. Lee • Y. Y. Su - "Aerodynamic performance of a wing with a deflected tip-mounted reverse half-delta wing". Exp Fluids (2012) 53:1221–1232 DOI 10.1007/s00348-012-1352-y*
36. *Thomas E Stimson Jr (1956) 'Era of flying Triangles' Popular Mechanics Vol. 106, No. 3 ISSN 0032-4558 Published by Hearst Magazines pp.63*
37. *van Dam, C. P., Nikfetrat, K., Wong, K., and Vijgen, P. M. H. W., "Drag Prediction at Subsonic and Transonic Speeds Using Euler Methods," Journal of Aircraft, Vol. 32, No. 4, pp. 839-845.*